Available online at www.sciencedirect.com
SCIENCE DIRECT®
Journal of Power Sources 118 (2003) 375–383
JOURNAL OF POWER SOURCES
www.elsevier.com/locate/jpowsour

Energy balance model of a SOFC cogenerator operated with biogas

Jan Van herle*, F. Maréchal, S. Leuenberger, D. Favrat

Laboratory for Industrial Energy Systems (LENI), Faculty of Engineering, Swiss Federal Institute of Technology (EPFL), CH-1015 Lausanne, Switzerland

Abstract

A small cogeneration system based on a Solid Oxide Fuel Cell (SOFC) fed on the renewable energy source biogas is presented. An existing farm biogas production site (35 m^3 per day), currently equipped with a SOFC demonstration stack, is taken for reference. A process flow diagram was defined in a software package allowing to vary system operating parameters like the fuel inlet composition, reforming technology, stack temperature and stack current (or fuel conversion). For system reforming simplicity, a base case parameter set was defined as the fuel inlet of 60% CH_4:40% CO_2 mixed with air in a 1:1 ratio, together with 800 °C operating temperature and 80% fuel conversion. A model stack, consisting of 100 series elements of anode supported electrolyte cells of 100 cm^2 each, was calculated to deliver 3.1 kW_{el} and 5.16 kW_{th} from an input of 1.5 N m^3/h of biogas (8.95 kW LHV), corresponding to 33.8 and 57.6% electrical and thermal efficiencies (Lower Heating Values (LHVs)), respectively. The incidence on the efficiencies of the model system was examined by the variation of a number of parameters such as the CO_2 content in the biogas, the amount of air addition to the biogas stream, the addition of steam to the fuel inlet, the air excess ratio λ and the stack operating temperature, and the results discussed.

Keywords: Biogas fuel; SOFC stack model; Energy balance; Efficiency

1. Introduction

Biogas fuel, despite attractive advantages of being indigenous, local, versatile and renewable, remains a largely underexploited energy source. Solid Oxide Fuel Cell (SOFC) cogenerators, owing to their modularity and relative insensitivity to microcontaminants that biogas may contain, could substantially upgrade the value of this fuel. The number of SOFC units in the 5–500 kW range that can be installed on farms, landfill sites, sewage treatment plants, organic solid waste digesters or organic liquid effluent treatment sites is potentially enormous [1].

An example of a SOFC-biogas combined small heat and power system is considered here. An existing family-farm site (located in Lully, Switzerland) produces biogas from livestock (20 cattle units) at a current typical rate of 35 m^3 per day, sufficient to satisfy the electrical and heating needs for the entire estate. Normally equipped with a small cogeneration gas engine (5 kW_{el}, electrical efficiency 17% and thermal efficiency 73%, Lower Heating Values (LHVs)), a Sulzer HEXIS SOFC module (1 kW_{el} class) has recently been taken in operation on the site, for demonstration and investigation purposes [2,3].

The present document performs the energy balance analysis on such a system, in order to assess conversion efficiencies of biogas by SOFCs, as a function of the variation of adjustable operating parameters such as reforming conditions, air excess rate, SOFC stack temperature, imposed stack current (equivalent to the fuel conversion rate), etc.

In order to exploit the site with a single stack, a number of modifications are proposed in the model with respect to the stack operated on site (limited to 1 kW_{el}, whereas the site produces around 9 kW_{total}). These simple modifications are the increase in cell number (from 50 in the existing unit to 100 in the model unit) and the improvement of single cell performance in the model, by choosing anode supported electrolyte cell technology instead of electrolyte supported cells (installed on site). The former can deliver double the performance of the latter, at similar temperature levels.

The installed reformer technology on site is the same as that used for natural gas, i.e. steam reforming (Eq. (1)) at a steam-to-carbon ratio of 2. In the model, partial oxidation reforming (Eq. (2)) with air (POX) will mainly be considered as alternative option, for reasons of balance-of-plant simplicity.

$$CH_4 + H_2O \Leftrightarrow 3H_2 + CO \quad (1)$$

* Corresponding author. Tel.: +41-21-693-35-10; fax: +41-21-693-35-02.
E-mail address: jan.vanherle@epfl.ch (J. Van herle).

0378-7753/03/$ – see front matter © 2003 Elsevier Science B.V. All rights reserved.
doi:10.1016/S0378-7753(03)00103-4

$$CH_4 + \tfrac{1}{2}O_2 \Rightarrow 2H_2 + CO \quad (2)$$

2. System model

2.1. Process flow model

A schematic overview of the considered system is depicted in Fig. 1. Freely adjustable input parameters are indicated in bold in the figure. "*Q*" represents exchanged heating power (in kJ/s or kW), "*W*" represents mechanical or electrical power (kW).

The biogas input is considered as a mixture of methane, CH_4, and carbon dioxide, CO_2, the total flow of which is fixed (N m^3/h) and the ratio of which can be chosen (usually 60% CH_4:40% CO_2 by volume). Reforming agents, either water or air, or both, can be added to the biogas, in adjustable quantities (ratio S:C, steam-to-methane ratio, and ratio air flow:biogas flow (v/v)). This necessitates knowledge of the actual methane content in the biogas stream. On site, the biogas composition (analysis of CH_4, CO_2 and H_2S contents) is continuously monitored.

Biogas and oxidant air can be chosen to be compressed; in reality, for a very small system as the one considered here, only blowers are installed, to give inlet pressures of 1.05–1.1 bar. Owing to process flow definition, *W*1 and *W*2 take account of steam compression (flux "9") as well, when required.

All fuel side inlet streams are preheated to reformer temperature, mixed and reacted over a reformer catalyst (in this case located close to the hot fuel cell stack), at a fixed temperature, $T_{reformer}$. The reformer outlet stream (number "11" in Fig. 1) is then finally, when necessary, further brought to the stack operating temperature level, T_{stack}, as anode zone inlet.

The air flow circulated to the cathodes is determined by the chosen air excess ratio, λ, taking into account the air already mixed with the fuel for partial oxidation reforming (stream "4", determined by the chosen air:biogas ratio). "Air" is defined as the mixture of 0.79 N_2/0.21 O_2 at 60% relative humidity. It is preheated to stack temperature (15) where it is separated into (i) the oxygen stream (16) passing through the solid electrolyte to the anode zone and (ii) the cathode exit or air excess stream (17).

The SOFC stack itself is represented by a reactor combining the reformer outlet stream (12) and the permeated oxygen stream from the cathode (16), to produce the anode outlet stream (18). The reactions considered to take place in this reactor are steam reforming (Eq. (1), at equilibrium), water gas shift (Eq. (3), equilibrium) and fuel oxidation (Eq. (4), conversion, i.e. elimination of all oxygen):

$$CO + H_2O \Leftrightarrow H_2 + CO_2 \quad (3)$$

$$CO + H_2 + O_2 \Rightarrow H_2O + CO_2 \quad (4)$$

The isothermal stack (T_{stack}) produces electrical dc power and heat (*Q*9 in Fig. 1).

Anode outlet (18) and cathode outlet (17) are combined in a post-combustion zone, where the remaining fuel fraction $(1 - u_f)$ is converted to products. The post-combustor

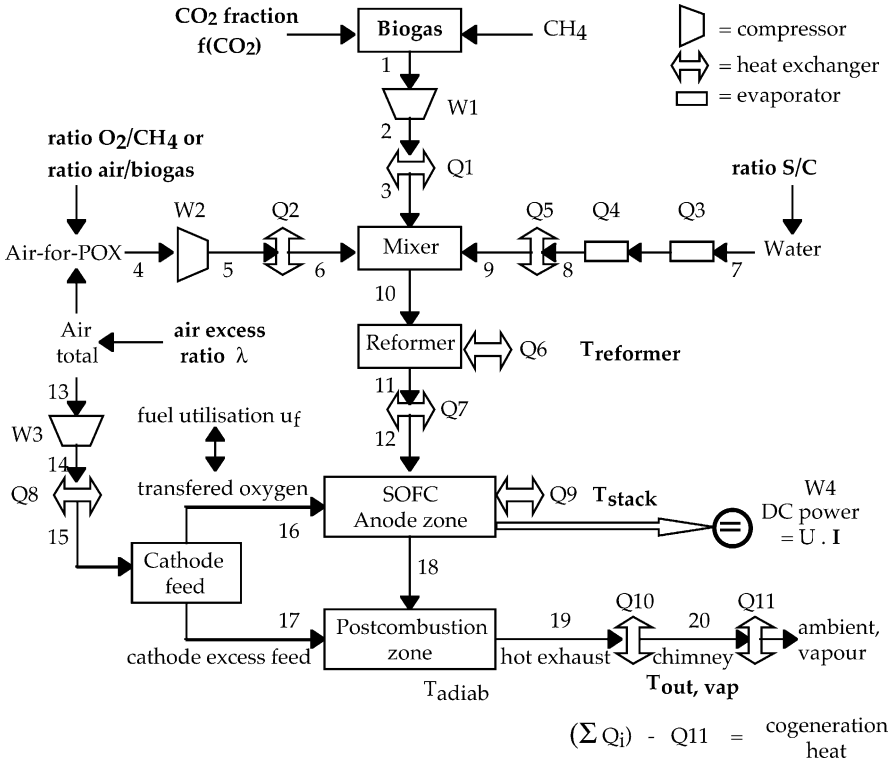

Fig. 1. Process flow diagram of the considered SOFC system fed on biogas mixtures.

is therefore defined as a mass balance reactor where all carbon and hydrogen species are present only in the final form of CO_2 and H_2O, respectively. The heat liberated in this zone is allowed to be transferred to the exhaust, giving raise to an equivalent "T_{adiab}" (Fig. 1), or highest system exhaust temperature, which is a computed value. The total heat available in this exhaust is recovered in $Q10$ (cooled down to the temperature and state "$T_{out,\ vap}$", e.g. 90 °C vapour, of the chimney reject stream "20") and $Q11$, the heat flux in the chimney reject stream with respect to the environment (15 °C, 1 bar, vapour state). The same conditions (15 °C, 1 bar) are chosen at all inlet streams, allowing to perform the energy balance (LHV) on the system cycle. The balance of all heat sources (here: $Q9$, $Q10$, $Q11$) and heat sinks (here: $Q1$ to $Q8$), subtracted by the heat released to the environment ($Q11$), allows to obtain the cogeneration heat available. The latter value, as well as the electrical power from the stack, is related to the fuel input (LHV of methane in biogas) to obtain the cogeneration thermal and electrical efficiency values (%), respectively. The latter, ε_{ELEC}, is corrected for the mechanical power used in compression (blowers $W1$ to $W3$) to obtain net dc efficiency. The former, ε_{COGEN}, should in principle be corrected for heat loss of the system to the environment; these have been estimated by convection and radiation to amount to below 1% for a well-insulated system [4], so are not considered here. "Ideal" cogeneration thermal efficiency (LHV) is thus reported.

2.2. Electrochemical model

The stream of oxygen transferred through the electrolyte from cathode to anode (16) is determined by the fuel utilisation, which could be chosen as a fixed value. Alternatively and equivalently, the imposed stack current can be chosen, with the fuel utilisation then computed based on the fuel input, using Faraday's law. This situation corresponds to the operation reality of a fuel cell, where the output current is directly controllable rather than the fuel utilisation. The unknown oxygen and air streams (mol/s) "4", "13", "16" and "19" are obviously strongly interrelated and calculated by the following set of simultaneous equations:

$$\text{"16"}(\text{transfered O}_2, \text{mol/s}) = \frac{I_{stack} \cdot N_{cells}}{4F} \tag{5}$$

$$\begin{aligned}\text{"4"}(\text{airflow fuel side, mol/s}) &= \text{"1"} \cdot r_{air/biogas} \\ &= \text{"1"} \cdot r_{O_2/CH_4} \frac{1 + (0.79/0.21)}{1 + (f_{CO_2}/(1 - f_{CO_2}))}\end{aligned} \tag{6}$$

$$\begin{aligned}\text{"13"} - \text{"19"}(\text{stoichiometric O}_2, \text{mol/s}) \\ = \frac{\text{"16"}}{u_f} = 2(1 - f_{CO_2}) \cdot \text{"1"} + \text{"7"} - \text{"4"}\end{aligned} \tag{7}$$

$$\lambda(\text{air excess value}) = \frac{\text{"4"} + \text{"13"}}{\text{"4"} + (\text{"13"} - \text{"19"})} \tag{8}$$

Electrical power output from the stack is calculated from the available Gibbs free enthalpy flow (kW), from which the irreversible losses are subtracted:

$$\text{electrical dc power} = (-\Delta \dot{G}_{stack}) - \text{electrical losses} \tag{9}$$

$$\Delta \dot{G}_{stack} = (\dot{G}_{18} + \dot{G}_{17}) - (\dot{G}_{15} + \dot{G}_{12}) = \dot{G}_{18} - (\dot{G}_{16} + \dot{G}_{12}) \tag{10}$$

$$\begin{aligned}&\text{electrical losses} \\ &= R_{ohmic,stack} \cdot I_{stack}^2 + (\eta_{cathode} + \eta_{anode}) \cdot N_{cells} \cdot I_{stack}\end{aligned} \tag{11}$$

In Eq. (11), a differentiation between total ohmic loss and non-ohmic losses (electrode polarisation η), at the cathode and anode interfaces, was made. The latter are obtained from empirical expressions, fitted to experimental current overpotential data measured individually on the cathode and anode materials, and which resemble Butler–Volmer equations:

$$\begin{aligned}j &= j_{0,anode}\left[\exp\left(\frac{2F}{RT}\eta_{anode}\right) - \exp\left(-\frac{F}{RT}\eta_{anode}\right)\right] \\ j &= j_{0,cathode}\left[\exp\left(\frac{F}{2RT}\eta_{cathode}\right) - \exp\left(-\frac{F}{2RT}\eta_{cathode}\right)\right]\end{aligned} \tag{12}$$

with

$$\begin{aligned}j_{0,anode} &= \frac{RT\sigma_{anode}}{3F}, \quad \sigma_{anode} = \sigma_{0,anode} \cdot \exp\left(-\frac{E_{A,anode}}{RT}\right) \\ j_{0,cathode} &= \frac{2RT\sigma_{cathode}}{F}, \quad \sigma_{cathode} = \sigma_{0,cathode} \cdot \exp\left(-\frac{E_{A,cathode}}{RT}\right)\end{aligned} \tag{13}$$

and where the pre-exponential factors σ_0 and the activation energies E_A are empirical constants.

Ohmic losses are obtained as a sum of the in-house empirically measured loss ($\Omega\ cm^2$) at the metallic interconnect-anode (R_{ICA}) contact and interconnect-cathode (R_{ICC}) contact, as well as the specific ohmic single cell resistance ($\Omega\ cm^2$). The first two (R_{ICA}, R_{ICC}) vary little as a function of temperature and are thus taken as constant. The third is taken from the known (and in-house measured) Arrhenius relation of the 8YSZ (yttria-stabilised zirconia) electrolyte resistivity,

$$\sigma_{8YSZ-electrolyte} = \sigma_{0,8YSZ-electrolyte} \cdot \exp\left(-\frac{E_{A,8YSZ-electrolyte}}{RT}\right) \tag{14}$$

corrected by a current collection factor f_{CC} [5,6], taken here as a constant (amounting to 4). We find indeed consistently that the measured ohmic loss on single cells of anode supported electrolyte SOFC, are about a factor 3–5 larger than the value expected from the electrolyte resistivity alone [7], owing to the geometry of current collection.

Table 1
Cell parameters and empirical electrochemical constants used in Eqs. (11)–(15)

Parameter	Symbol	Value
Cell number	N_{cells}	100
Cell area	A	100 cm^2
Pre-exponential factor	σ_0, anode	433033 S/cm
Pre-exponential factor	σ_0, cathode	61527821 S/cm
Pre-exponential factor	σ_0, electrolyte	372.33 S/cm^2
Activation energy	E_A, anode	115781 J/mol
Activation energy	E_A, cathode	157659 J/mol
Activation energy	E_A, electrolyte	79535 J/mol
Current collection correction factor	f_{CC}	4
Contact loss interconnect-anode	R_{ICA}	0.03 Ω cm^2
Contact loss interconnect-cathode	R_{ICC}	0.10 Ω cm^2

We therefore have:

$$R_{cell}(\Omega\,cm^2) = R_{ICA} + R_{ICC} + f_{CC} \cdot R_{8YSZ-electrolyte}$$
$$R_{ohmic,stack} = \frac{R_{cell} \cdot N_{cells}}{\text{cell area (cm}^2)} \quad (15)$$

Values for all the constants used in the relations (11)–(15) are summarised in Table 1.

The final two useful values obtained from the algorithm are the cell operating voltage U_{cell} and current density j,

$$j\,(A/cm^2) = \frac{I_{stack}}{\text{cell area}} \quad (16)$$

$$U_{cell} = \frac{U_{stack}}{N_{cells}}, \quad \text{where} \quad U_{stack} = \frac{\text{electrical dc power}}{I_{stack}} \quad (17)$$

3. Experimental

The algorithm was implemented into the software package, VALI^{TM}, from the company BELSIM SA (Liège, Belgium). VALI^{TM} is a data reconciliation programme originally developed for the chemical process industry. The system depicted in Fig. 1 is entirely defined by a set of 134 equations. For the purpose of the present system study, VALI^{TM} was here furthermore interfaced with MATLAB^{TM}, to allow to specify a variation range of a specific operating parameter with a discrete increment; the resulting system output is then calculated for each incremental value of the varied input parameter in each iteration, and stored in an output file for graphical consultation. Typical input variables for the considered system (indicated in bold in Fig. 1) were the air:biogas ratio in the fuel (degree of POX reforming), the biogas CO_2 content, the air excess ratio λ, the reformer and stack temperatures, and the stack operation current. The output parameters of interest were the (net) electrical ε_{ELEC} and (ideal) thermal cogeneration efficiency ε_{COGEN}, the various exchanged heat fluxes Q, and the gas composition at different locations in the process flow.

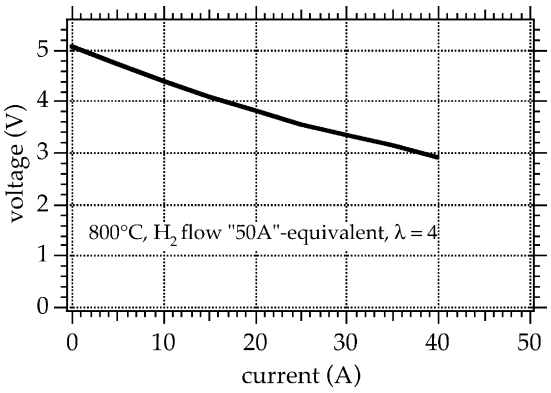

Fig. 2. Experimental characteristic of anode supported electrolyte five-cell stack with H_2 fuel at 800 °C, showing no evidence of mass transfer limitation up to 80% fuel conversion ($\varepsilon_{ELEC} = 34\%$).

The present model shows a number of shortcomings, the first one being the assumption of isothermal reformer and stack operation. In reality, these subunits can cool or heat locally owing to kinetics and thermal inertia. Second, no diffusion overpotential (or current limitation due to mass transfer) was taken into account (like, e.g. in [8]). These simplifications will be corrected in a more improved model in future. Nevertheless, experimental short-stack results with our anode supported electrolyte cells have shown outputs on the order of 0.25 W/cm^2 at 800 °C up to at least 80% fuel conversion, u_f, without any sign of mass transfer limitation (Fig. 2).

An example of the biogas composition monitored on site where the SOFC demonstration stack is operated is given in Fig. 3. It appears that for such a small, family-operated installation, where organic substrate is filled batchwise in one of four digesters connected in parallel to the biogas production line, the composition may vary substantially. In particular, it is evident how after filling of a new batch (one of the four digesters opened, filled with substrate, and closed again), air intake into the gas mixture lowers the methane and carbon dioxide content simultaneously (day 92 on

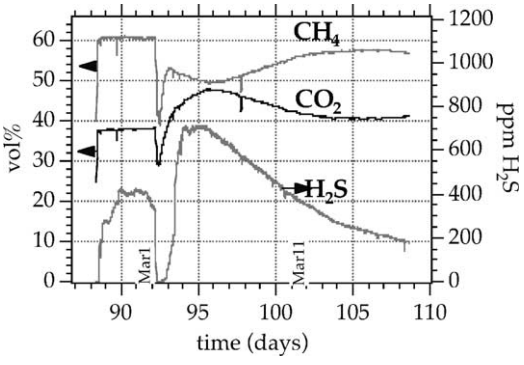

Fig. 3. Biogas composition variation monitored on-line at a Swiss farm site, where an SOFC demonstration system is operated.

Table 2
Measured averaged biogas compositions of different production sites (Switzerland)

Site	Type	CH_4 (vol.%)	CO_2 (vol.%)	$O_2 + N_2$ (vol.%)	H_2S (ppm)
1	Farm	57.0	41.0	2	100
2	Farm	62.9	36.1	1	200
3	Sewage	64.5	34.5	1	<2
4	Sewage	61.5	38.3	0.2	<1

stream in Fig. 3), to recover after about 1 day. Simultaneously, an important transient in H_2S is observed, reaching a peak of 700 ppm (owing to fresh liquid manure added from the farm animals) to only very slowly (2 weeks) be reduced to around 100 ppm, which was the typical content in stable operation, until the next batch refill. Averaged over a current monitoring period of 7 months, CH_4 content averages out to around 57% for this particular site.

For other, larger sites (100 kW_{el}), in particular sewage treatment plants, composition is both more stable and richer in methane (Table 2).

4. Results

To assess the behaviour of the generic SOFC-biogas system schematically drawn in Fig. 1, in particular the efficiencies as a function of input parameters accessible by a fuel cell system operator, a base model case or reference case was defined. The fixed input parameters of this base model case are given in Table 3, together with the range over which one such parameter was varied while keeping all others constant as in the base case.

The base case model parameter set was chosen for the condition where reforming of average biogas (60–40% CH_4–CO_2, see Table 2) with an equal volume flow of air (1.5 N m^3/h), i.e. $r_{O_2/CH_4} = 0.21/0.6 = 0.35$, is free of carbon deposition risk. Under these conditions, the thermodynamical limit of carbon formation (graphite) from the mixture lies at around 740 °C. The fuel input of 1.5 N m^3/h corresponds roughly to the actual farm biogas production on site (35 m^3 per day at 15 °C).

For the base case, the obtained system output parameters are given in Tables 4 and 5.

5. Discussion

5.1. Reference case

Fig. 4 displays the stack electrical output, as a function of current, of the model system. Resemblance to the slope and shape of the experimental voltage–current behaviour using anode supported electrolyte cells (Fig. 2) is satisfactory, the main difference lying in the open circuit voltage (OCV). Indeed, the model assumes perfectly sealed cells whereas the measurement from Fig. 2 was effectuated in a seal-less set-up, leading to an OCV per cell about 0.05 V below the theoretical value. Net electrical dc efficiency amounts to 33.8% at 80% fuel utilisation, for the model system. Existing Sulzer HEXIS 1 kW_{el} systems, operated on natural gas, presently reach an electrical efficiency of 35% (dc, LHV) [9]. Cogeneration thermal efficiency (ε_{COGEN}) varies in opposite fashion to the electrical efficiency (ε_{ELEC}), from 91.4% (zero current) down to 57.6% (55 A). Total efficiency ($\varepsilon_{COGEN} + \varepsilon_{ELEC}$) remains constant at 91.5%, the 8.5% loss corresponding to the heat flux sent up the chimney to the environment (−0.77 kW).

A comment to the "Gibbs cell voltage" V_G (Table 4), 0.987 V, is useful, in order to avoid confusion with the Nernst voltage, E. From Table 4, we see that the Gibbs free enthalpy flow of the stack reaction (Eq. (10)) amounts to $-3.117 - 2.494\,kW = -5.611\,kW$. This is brought in relation to the cell voltage by

$$V_G = \frac{-(\Delta \dot{G}_{stack}/N_{cells})[W]}{nF[C/mol] \cdot (\text{fuel flow}[mol/s]/N_{cells})[A]} \quad (18)$$

Table 3
Variable system parameters, with indication of the value set chosen for a reference case, and of the value range for input parameter variation while keeping all others constant

Parameter	Symbol	Base case	Range
Fuel input	"1"	1.5 N m^3/h	Constant
Gas streams inlet temperature	"1", "4", "7", "13"	15 °C	Constant
Carbon dioxide content in biogas	f_{CO_2}	0.4	0.2–0.65
Steam-to-methane ratio	$r_{S/C}$	0	0–2
Oxygen-to-methane ratio (POX)	r_{O_2/CH_4}	0.35	0.3–0.6
Reformer temperature	$T_{reformer}$	800 °C	700–800 °C
Stack temperature	T_{stack}	800 °C	700–1000 °C
Air excess ratio	λ	3	1–7
Fuel utilisation	u_f	0.8	Calculated
Stack operating current	I_{stack}	u_f "1" = 57 A	0–60 A
Exhaust reject state	$T_{out,\ vap}$	90 °C, vapour	Constant
Gas inlet pressures	P	1.05 bar	1–3 bar

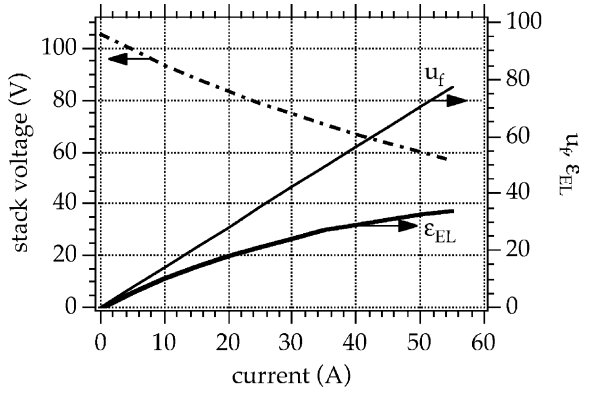

Fig. 4. Electrical output of the biogas-fed SOFC system, using the reference case parameter set from Table 3 as input.

The fuel flow (in mol/s) is obtained from the biogas flow (1.5 N m^3/h), the methane fraction (0.6) and the conversion factor from N m^3/h to mol/s (1 mol = 22.4 l), to give 111.52 mmol CH_4 per cell in the 100-cell stack. The correct charge number, n, which would be 8 for pure CH_4 ($8F$ mole electrons exchanged per mole of CH_4 fuel) is obtained from the considerations that (i) part of the CH_4 fuel inlet is already chemically converted by the POX reaction in the reformer, and that (ii) only the fraction u_f (0.8) of this converted fuel is actually available for transformation to electrical current. The first correction factor is obtained from the O_2:CH_4 ratio in the inlet mixture: this ratio being 2 for full conversion (total oxidation to CO_2, $n = 0$), and 0.35 for the present fuel mixture (Table 3, base case), the correction is given by $(2 - 0.35)/2 = 0.825$. In other words, an electrical current efficiency drop of 17.5% with respect to pure CH_4 or pure biogas feed (without air addition) is inherent with the chosen inlet composition. The equivalent charge number n from Eq. (18) thus amounting to $8 \times 0.825 \times 0.8 = 5.28$, we confirm the value for V_G as

$$V_G = \frac{56.11\,\mathrm{W}}{(5.28F \times 0.00011152)\,\mathrm{A}} = 0.987\,\mathrm{V}$$

On the other hand, the Nernst voltage is obtained from considering the Gibbs free enthalpy from the stoichiometric combustion reaction

$$CH_4 + H_2 + CO + 3O_2 \rightarrow 3H_2O + 2CO_2 \qquad (19)$$

for which ΔG° (800 °C) is calculated from standard thermodynamic data-tables to −1178.2 kJ/mol. This leads to a standard Nernst potential for this reaction of $\Delta G^\circ/12F$ (12 electrons exchanged in reaction (19)) or 1.018 V. The cell potential, E, at non-standard concentrations is then calculated by considering

$$\Delta G_{\mathrm{total}} = \Delta G^\circ_{\mathrm{total}} + RT \ln K \quad \text{or} \quad E = E^\circ + \frac{RT}{12F} \ln K^{-1}$$

where

$$K^{-1} = \frac{p_{CH_4,\mathrm{anode}} \cdot p_{H_2,\mathrm{anode}} \cdot p_{CO,\mathrm{anode}} \cdot p^3_{O_2,\mathrm{cathode}}}{p^3_{H_2O,\mathrm{anode}} \cdot p^2_{CO_2,\mathrm{anode}}} \left(\frac{1}{p^0}\right)^1 = \frac{c_{CH_4} \cdot c_{H_2} \cdot c_{CO} \cdot c^3_{O_2}}{c^3_{H_2O} c^2_{CO_2}} \left(\frac{p}{p^0}\right)^1 \qquad (20)$$

Taking the proper molar fractions at anode (Table 5) and cathode side ($c_{O_2,\mathrm{cathode\,inlet}} = 0.21$, $c_{O_2,\mathrm{cathode\,outlet}} = 0.21(1 - u_f/\lambda)$) for the relevant species produces then cell equilibrium voltages, e.g. of 1.041 V at open circuit and of 0.865 V at 80% utilisation. Note that the latter value is

Table 4
Output parameters for the SOFC-biogas system, considering the reference case

Parameter	Symbol	Value
Inlet fuel energy flow (LHV)	Flux "1"	8.947 kW
Stack voltage	U_{stack}	54.85 V (0.5485 V per cell)
Stack current	I_{stack}	56.82 A (0.5682 A/cm^2)
Stack power	ELEC	−3.117 kW (0.312 W/cm^2)
Total compressor work	$W1 + W2 + W3$	0.094 kW
Net electrical efficiency	$\varepsilon_{\mathrm{ELEC}}$	33.79%
Anode overpotential	η_{anode}	0.135 V
Cathode overpotential	η_{cathode}	0.185 V
Ohmic loss	$R_\Omega \cdot I_{\mathrm{stack}}$	0.119 V ($R_\Omega = 0.21\ \Omega\,\mathrm{cm}^2$)
Gibbs cell voltage	V_G	0.987 V
Joule loss	$R_\Omega \cdot (I_{\mathrm{stack}})^2 + (\eta_a + \eta_c) I_{\mathrm{stack}} \cdot N_{\mathrm{cells}}$	−2.494 kW
Entropy loss	$T\,\Delta S$	−2.125 kW
Stack heat	$Q9$	−4.619 kW
Post-combustion temperature	T_{adiab}	960 °C
Hot exhaust heat flux	$Q10$	−9.894 kW
Chimney heat flux	$Q11$	−0.767 kW
Fuel pre-heater flux	$Q1$	+0.765 kW
Total air pre-heater flux	$Q2 + Q8$	+7.844 kW
Reformer heat flux (endotherm)	$Q6$	+0.744 kW
Total heat balance	ΣQ	−5.926 kW
Cogeneration thermal efficiency	$((\Sigma Q) - Q11)$/LHV	57.66%

Input parameter set as in Table 3, base case.

Table 5
Gas composition (mol%) at various locations in the system process flow

Location	CH_4	CO_2	H_2O	O_2	N_2	CO	H_2
Fuel inlet "10"	29.85	19.9	0.51	10.45	39.3	–	–
Reformer outlet "11"	0.225	3.63	4.30	–	26.45	29.62	35.77
Anode outlet "18"	–	27.41	33.06	–	26.33	5.92	7.28
System outlet "19"	–	5.46	7.51	13.10	73.93	–	–

distinct from the Gibbs voltage 0.987 V calculated above, obtained for 80% fuel conversion. The difference originates from the fact that in the former case (Nernst situation), the whole anode chamber corresponds to a product concentration of 80%, whereas in the latter case (Gibbs situation), only the anode outlet is subjected to a 80% product fraction.

5.2. Model output response to input parameter variation

In the following, parameter range variation with respect to the reference case is carried out, specified in Table 3.

Fig. 5 shows the variation in electrical efficiency, ε_{ELEC}, when varying the CO_2 fraction in the biogas feed between 20 and 65%, which are the extreme composition limits one may find for biogas. It is remarked that for CO_2 fractions above 55%, conventional engines will cease to operate, whereas SOFCs can easily handle dilute fuel. For the calculation in Fig. 5, the O_2-to-CH_4 ratio was kept constant at 0.35, and fuel utilisation at 0.8. Perhaps counter-intuitively, efficiency actually increases with poorer biogas (richer in CO_2), reaching a flat maximum at 60% CO_2 for the studied system. Explanation is given from the fact that, for richer biogas (higher CH_4 content, hence higher input LHV numbers), constant 80% fuel conversion leads to higher current, therefore to higher ohmic loss (RI^2) and lower operating voltage, as also shown in Fig. 5.

Fig. 6 shows the variation in electrical and thermal cogeneration efficiency upon changing the amount of air added to the biogas stream for partial oxidation. It is evident that ε_{ELEC} drops, but to a small extent (2% points when doubling the amount of added air), as more methane is chemically converted in the reformer by combustion, leaving less fuel available for electrical conversion on the SOFC stack. In the present case, the imposed stack current was left fixed at 50 A and the resulting fuel utilisation calculated, simulating the real case situation of a stack under constant load but experiencing air leakage in the biogas inlet (see, for example, Fig. 3). As the fuel sent to the stack becomes leaner with higher air fraction in the inlet, fuel conversion u_f, for constant current load of 50 A, rises and stack voltage drops

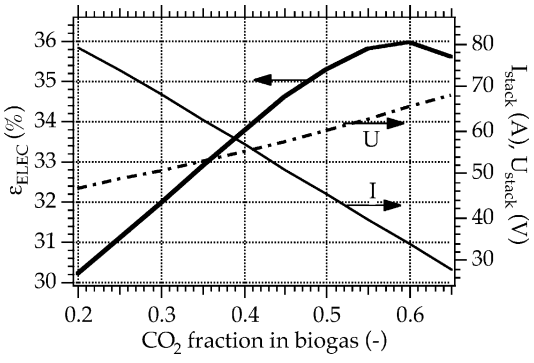

Fig. 5. Variation of electrical efficiency, stack current and stack voltage as a function of CO_2 content in the biogas feed.

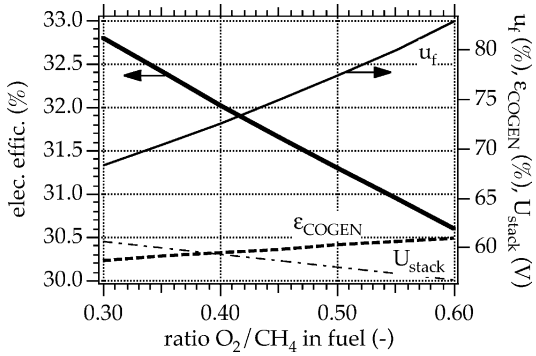

Fig. 6. Variation in electrical and cogeneration thermal efficiencies, fuel conversion and stack voltage, as a function of air addition to the biogas feed, for a constant stack load (50 A).

thermodynamically (higher content in oxygen species at the anode inlet).

Fig. 7 illustrates the effect of adding also steam to the fuel inlet. This approaches the real case situation, as the existing SOFC system on site is operated under steam reforming condition. Electrical efficiency ε_{ELEC} drops upon adding water because the thermodynamic voltage (OCV) drops, indicated in the figure by the reduction in stack voltage while fuel conversion (0.8) and stack current (56.8 A) remain constant. Cogeneration thermal efficiency ε_{COGEN} drops markedly with water addition as the evaporation heat consumed at the inlet is not recovered by the exhaust (no condensation). This differs from the operation with a water-free fuel inlet (for example, Fig. 6), where ε_{COGEN} rises as ε_{ELEC} drops. Total system efficiency is thus reduced from 91.5 to 80% when operating the 1:1 biogas:air feed on a steam-to-carbon ratio of 2.

Fig. 8 treats the case of steam reforming only, having removed air addition to the biogas inlet (the O_2:CH_4 ratio is set to 0). This is equivalent to the reforming conditions used on site. Electrical and cogeneration thermal efficiencies still follow the same decreasing trend with increasing S:C ratio as in Fig. 7, however, the electrical efficiency value is shifted upwards by about 3% points (compared to Fig. 7) whereas

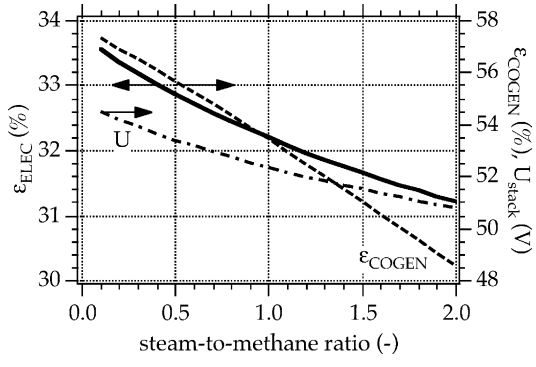

Fig. 7. Variation in electrical and cogeneration thermal efficiencies, as well as stack voltage, as a function of water addition to the 1:1 biogas:air feed, at constant load (u_f and I_{stack}).

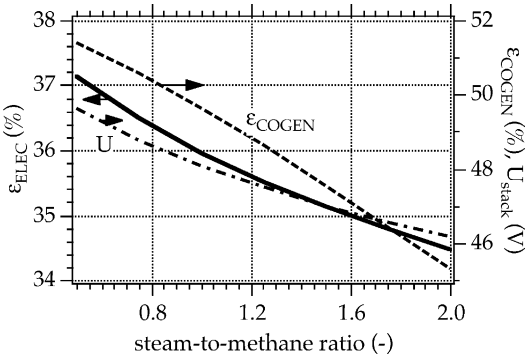

Fig. 8. Variation in electrical and cogeneration thermal efficiencies, as well as stack voltage, as a function of water addition to biogas (without air addition), at constant fuel conversion (0.8).

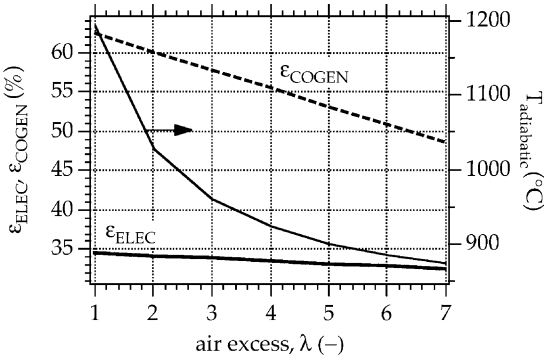

Fig. 10. Variation in electrical and cogeneration thermal efficiencies, and adiabatic temperature of the hot system exhaust (after post-combustion), as a function of air excess ratio λ, keeping all other parameters constant (base case, Table 3).

the cogeneration thermal efficiency value is shifted downwards by about 3% points (compared to Fig. 3). The raise in ε_{ELEC} originates from the fact that, at the same fuel conversion of 80%, current is substantially higher (68.9 A) than for the case where air is present in the fuel (56.8 A). This is again explained by the avoidance of fuel loss by chemical conversion (partial oxidation) in the reformer when no oxygen is added to the fuel. In fact, the electrical current ratio 56.8/68.9 A amounts to 0.825, exactly the correction factor obtained higher for the charge number n (=available fuel for electrical conversion) when calculating the Gibbs voltage.

Fig. 9 demonstrates the variation in electrical and cogeneration thermal efficiencies as a function of SOFC stack temperature between 750 and 1000 °C, at constant fuel inlet flow and fuel utilisation (0.8) while keeping the reformer temperature constant at the lowest limit of this temperature range (750 °C). Inlet conditions otherwise correspond again to the base case (1:1 biogas:air, 40% CO_2 in biogas, no water added). Evidently, owing to the thermally strongly activated electrode processes and electrolyte conductivity, electrical efficiency drops strongly between 850 °C (41.1%) and 750 °C (23.6%): to maintain constant current (57 A, constant fuel conversion, 80%), cell voltage drops drastically at lower temperature, also indicated in the figure. Electrical efficiency levels off at the highest temperatures: the gain obtained in lower cell electrical losses is diminished by the concurrent drop in thermodynamic cell voltage (OCV) at higher temperature.

Fig. 10 displays the effect of the used air excess ratio, λ, on resulting efficiencies of the biogas:air (1:1) cofeed system. Electrical efficiency should remain constant when operating at 1 bar. Since inlet pressures of 1.1 bar were used, more compression work is performed at higher air flow λ, slightly decreasing net electrical output. Obviously, cogeneration thermal efficiency drops substantially for higher λ, as more system heat is required to preheat the larger air mass to operating temperature. At the same time, heat recovery potential from the hot exhaust does not increase concomitantly owing to the cooling effect of the large air mass: this is indicated in the figure by the adiabatic temperature level in the post-combustion zone for varying λ. Not accounted for in Fig. 10 is the possible drop in electrical output, and therefore in ε_{ELEC}, at very low λ (1, or stoichiometric air ratio), due to an increase in cathode overpotential because of oxygen transfer limitation.

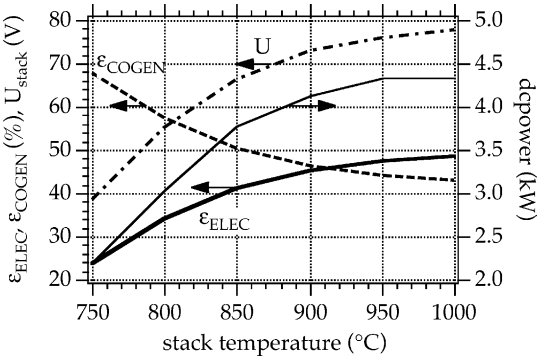

Fig. 9. Variation in electrical and cogeneration thermal efficiencies, as well as stack voltage and absolute electrical output, as a function of stack operating temperature (biogas:air 1:1, constant fuel conversion (0.8), reformer kept at 750 °C).

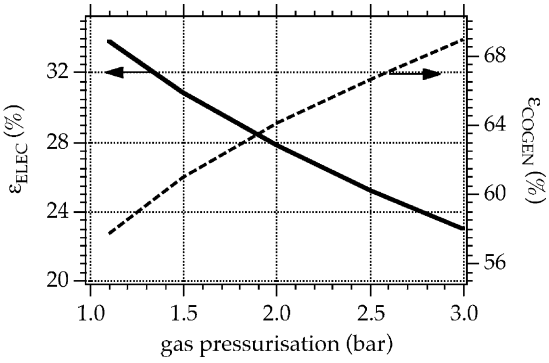

Fig. 11. Variation in electrical and cogeneration thermal efficiencies when pressurising the system (without recovery from an expansion turbine at the outlet).

Fig. 11, finally, illustrates the effect of pressurisation on resulting system efficiencies. Evidently for such a small system (9 kW_{total}), net electrical efficiency drops drastically upon pressurisation (and cogeneration heat efficiency rises concomitantly), more compression work being required at both inlets. Not yet taken into account in Fig. 11 is the recoverable mechanical work from expansion of hot exhaust in a turbine nor the compensating effect of lower electrode overpotentials due to improved mass transfer at higher pressures. As the reported [10] increase in cell voltage for pressurising from 1 to 3 bar amounts to 50–100 mV, the latter gain in electrical output will remain small compared to the higher compression loss.

6. Conclusion

A small cogeneration system based on a SOFC fed on a renewable energy source, biogas, was presented. An existing biogas production site (small farm, 9 kW_{total}), currently equipped with a 1 kW_{el} SOFC demonstration stack, was taken as starting point. A process flow diagram was defined in a software package allowing to vary system operating parameters like the fuel inlet composition, reforming technology, stack temperature and stack current (or fuel conversion). For system simplicity, a base case parameter set was defined as the fuel inlet of 60% CH_4/40% CO_2 mixed with air in a 1:1 ratio (corresponding to combined reforming), 800 °C operating temperature and 80% fuel conversion. A model stack, consisting of 100 series elements of anode supported electrolyte cells of 100 cm^2 each, was calculated to deliver 3.1 kW_{el} and 5.16 kW_{th} from an input of 1.5 N m^3/h of biogas (8.95 kW LHV), corresponding to 33.8 and 57.6% electrical and cogeneration thermal efficiency, respectively. This electrical output both in magnitude and efficiency compared well with experimental stack results obtained on such cells. The incidence on the efficiencies of the model system was examined by the variation of a number of operating parameters such as the CO_2 content in the biogas, the amount of air addition to the biogas stream, the addition of steam to the fuel inlet, the air excess ratio l and the stack operating temperature, and the results discussed.

A number of shortcomings of the present model were pointed out, such as the absence of reforming kinetics, the absence of electrode diffusion overpotential and the assumption of isothermally operated reformer and SOFC stack. These aspects will be corrected in an improved model in future. It is also planned to investigate and optimise the heat exchanger network of the considered system, by using composite curve theory and pinch analysis. Finally, the model can be extended to treat also the cases of other fuel cell types (molten carbonate MCFC operated at 650 °C, phosphoric acid PAFC at 200 °C and polymer electrolyte PEFC at 80 °C) supplied with biogas. Such systems will be of more important size (>100 kW_{el}) and therefore applicable to sewage and methanisation plants, landfill sites and large farms. Apart from the advantage with SOFCs in better tolerance to fuel contaminants (towards H_2S and other species), such a fuel cell type comparison will be likely to demonstrate also the overall better system performance of the high temperature SOFC type. Finally, exergy analysis will be carried out.

Acknowledgements

The company BELSIM SA is thanked for use of the software license of the programme VALI™. The Swiss Federal Energy Office is thanked for financial support (BFE Contract 79 385), as well as the partners of the SOFC biogas demonstration project (Sulzer HEXIS, A. Schuler, M. Jenne, EREP SA, Y. Membrez, V. Chabloz).

References

[1] J. Van Herle, Y. Membrez, Biogas exploitation in SOFC, in: U. Bossel (Ed.), Proceedings of the Fifth European Solid Oxide Fuel cell Forum, Lucerne, Switzerland, European Forum Secretariat, CH 5442-Oberrohrdorf, Switzerland, July 2002, pp. 1003–1010.

[2] M. Jenne, T. Zähringer, A. Schuler, G. Piskay, D. Moos, Sulzer HEXIS SOFC systems for biogas and heating oil, in: U. Bossel (Ed.), Proceedings of the Fifth European Solid Oxide Fuel Cell Forum, Lucerne, Switzerland, European Forum Secretariat, CH 5442-Oberrohrdorf, Switzerland, July 2002, pp. 460–466.

[3] J. Van herle, Y. Membrez, O. Bucheli, Biogas as a fuel source for SOFC cogenerators, J. Power Sources, in press.

[4] J. Van herle, SOFCs fueled with biogas, Masters Thesis in Energy Technology, Swiss Federal Institute of Technology (EPFL), 1015-Lausanne, Switzerland, Secretariat of the Laboratory for Energy Systems, 2001.

[5] J. Fleig, J. Maier, The influence of inhomogeneous potential distribution on the electrolyte resistance in SOFC, in: U. Stimming, S.C. Singhal, H. Tagawa, W. Lehnert (Eds.), Proceedings of the Fifth International Solid Oxide Fuel Cells Symposium, The Electrochemical Society Proceedings Series, Pennington, NJ, vols. 97/40, 1997, pp. 1374–1383.

[6] K. Nisancioglu, Ohmic losses in SOFC, in: Proceedings of the International Energy Agency (IEA) Workshop on Mathematical Modelling of Natural Gas Fuelled SOFC Systems, Charmey, Switzerland, Swiss Federal Energy Office (OFEN), CH-3003 Berne, Switzerland, July 1989.

[7] R. Ihringer, Electrolytes minces sur supports anodes dans les piles à combustible SOFC, Ph.D. Thesis, Swiss Federal Institute of Technology (EPFL), CH-1015 Lausanne, Switzerland, 2001.

[8] S.H. Chan, C.F. Low, O.L. Ding, Energy and exergy analysis of simple solid oxide fuel cell power systems, J. Power Sources 103 (2002) 188–200.

[9] H. Raak, R. Diethelm, S. Riggenbach, The Sulzer Hexis story: from demonstrators to commercial products, in: U. Bossel (Ed.), Proceedings of the Fuel Cell World, Lucerne, Switzerland, European Forum Secretariat, CH 5442-Oberrohrdorf, Switzerland, July 2002, pp. 81–88.

[10] S. Singhal, Recent progress in tubular SOFC technology, in: U. Stimming, S.C. Singhal, H. Tagawa, W. Lehnert (Eds.), Proceedings of the Fifth International Solid Oxide Fuel Cells Symposium, The Electrochemical Society Proceedings Series, Pennington, NJ, vols. 97/40, 1997, pp. 37–50.